

Cerebellar Pathways in Mouse Model of Purkinje Cell Degeneration Detected by High-Angular Resolution Diffusion Imaging Tractography

Yuri Kanamaru¹ · Jianxue Li² · Natalie Stewart³ · Richard L. Sidman² · Emi Takahashi^{4,5,6}

Published online: 19 January 2017
© Springer Science+Business Media New York 2017

Abstract Cerebellar MR imaging has several challenging aspects, due to the fine, repetitive layered structure of cortical folia with underlying axonal pathways. In this MR study, we imaged with high-angular resolution diffusion imaging (HARDI) abnormal cerebellar cortical structure (gray matter) and myelinated axonal pathways (white matter) of a mouse spontaneous mutation, *Purkinje cell degeneration (pcd)*, in which almost all Purkinje neurons degenerate, mainly between postnatal days 20 and 35. Mouse brains at postnatal day 20 (P20) and at 8 months were scanned, and known or expected abnormalities, such as reduction of the white matter volume, disorganized pathways likely linked to parallel fibers, mossy fibers, and other fibers running from/to the cerebellar cortex were observed in mutant mice. Such abnormalities were detected at both an early and a fully advanced degeneration stage. These results suggest that our diffusion MR

tractography is useful for early detection and tracking of neuropathology in the cerebellum.

Keywords Purkinje cell · Cerebellum · Development · Degeneration · Diffusion imaging · Tractography

Introduction

Purkinje neurons (PNs) in the cerebellar cortex, the ultimate target of all inputs to, and the sole source of outputs from the cerebellar cortex, play important roles in motor learning and coordination, as well as in several types of cognitive information processing [1–3]. PNs are still in a very immature form at birth in mice and humans but come postnatally to form the most elaborate dendritic trees of all neurons, with elaborate synaptic inputs from climbing fibers that originate from inferior olivary neurons in the medulla (ventral to the cerebellum) and parallel fibers from granule cell neurons within the cerebellar cortex, the most numerous neurons in the entire nervous system [4]. PNs are vulnerable neurons in various neurological diseases ranging from specific genetic defects to acquired injury or poisoning, including autism and Alzheimer’s disease [2, 5, 6]. Although several genetic and environmental factors impair PNs, the pathological mechanisms remain almost entirely undefined [7]. The nine *Purkinje cell degeneration (pcd)* mutations affect the *Nnal* (neuronal nuclear protein induced by axotomy) gene [8], to give a phenotype with impaired PN dendritic growth, followed by PN death, beginning at about postnatal day (P) 10 and degeneration of almost all PNs at P22–P35, followed by slower degeneration of many olfactory bulb mitral neurons, selected thalamic neurons, and retinal photoreceptor neurons [9]. In this study, we relied on past findings on abnormal brain size, cell structures, and fiber pathways in the *pcd* mutant mouse model [10] and qualitatively

✉ Emi Takahashi
emi@nmr.mgh.harvard.edu

¹ Department of Medicine, Chiba University School of Medicine, Chiba, Japan

² Department of Neurology, Beth Israel Deaconess Medical Center, Harvard Medical School, Boston, MA, USA

³ Department of Behavioral Neuroscience, Northeastern University, Boston, MA, USA

⁴ Division of Newborn Medicine, Department of Medicine, Boston Children’s Hospital, Harvard Medical School, Boston, MA, USA

⁵ Fetal-Neonatal Neuroimaging and Developmental Science Center, Boston Children’s Hospital, Harvard Medical School, 1 Autumn St. #456, Boston, MA 02115, USA

⁶ Athinoula A. Martinos Center for Biomedical Imaging, Massachusetts General Hospital, Harvard Medical School, Charlestown, MA, USA

showed how diffusion tractography can identify fiber pathway in the brain in accordance with the past findings. Li et al. [10] showed that in adult *pcd* mice (P120), all Purkinje neurons had degenerated and their axons had disappeared (Fig. 1a), resulting in reduced cerebellar white matter (Fig. 1b). In young mice (P20), PN dendrites in *pcd* mice were decreased in volume and branching, but the axon problem was not yet obvious when detected by regular immunostaining (Fig. 1c).

Diffusion MR tractography is useful for identifying pathways in the whole brain in 3D. High-angular resolution diffusion imaging (HARDI) tractography enables identification of complex crossing tissue coherence in the brain [11], even in very immature brains [12, 13], which are typically more challenging to reconstruct because most axons are still unmyelinated. This study used

HARDI tractography in an attempt to identify degeneration of fiber pathways in the cerebellum. In our previous tractography study on normal human brains, we successfully identified multiple different components of cerebellar fiber pathways at developing ages [14] and in adults [15]. We found that, in the cerebellar cortex, tractography detected tangential coherence superficially in the cerebellar cortex and revealed axonal fibers coursing parallel to the long axis of the folia and thus consistent with the location and orientation of parallel fibers in the molecular layer. Crossing these parallel fibers were tangential fibers running perpendicular to the long axis of the folia, consistent with axons of the cortical interneurons (mainly stellate cells). Our results demonstrated coherent tractography fiber structure likely reflecting the axonal pathways that characterize different cell types within the cerebellar cortex. In this study, we aim to show that our technique also detects degeneration of fiber pathways in the brain. Degeneration of fiber pathways in the *pcd* mouse brain has been well described in previous studies (e.g., [10]).

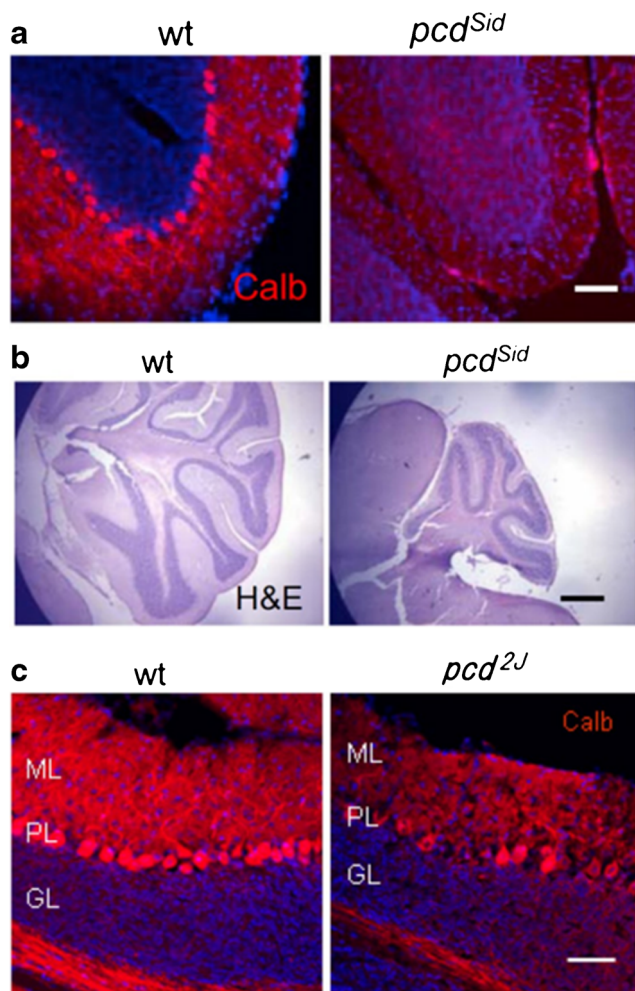


Fig. 1 Characterization of cerebellar histopathology and *Nnal* mutation in *pcd^{Sid}* mutant mice (a, b) and in a *pcd^{2J}* mutant (c) (from [10], permission obtained to reproduce in this paper). **b** Hematoxylin and eosin (H&E)-stained sagittal section showed an atrophic cerebellum in P120 *pcd^{Sid}* mutant. Scale bar represents 500 μ m. **a** Calbindin (Calb)-stained Purkinje cells (red) were totally lost in P60 *pcd^{Sid}* cerebellar cortex. Scale bar represents 50 μ m. **c** Calb-staining (red) showed abnormal Purkinje cell dendrites in P20 *pcd^{2J}* cerebellar cortex. ML molecular layer, PL Purkinje cell layer, GL granule cell layer. Scale bar 50 μ m

Methods

Animals

All procedures were in accordance with NIH-approved institutional guidelines maintained by the Institutional Animal Care and Use Committee of Harvard Medical School and the University of Connecticut. In this study, based on past histopathologic findings already published, we qualitatively assessed diffusion MR tractography pathways in two mutant (one at postnatal 20 days old and one at 7–8 months old) and two age-matched control mouse brains. Breeders of wild-type C57BL/6J mice were obtained from The Jackson Laboratory (Bar Harbor, ME, USA). We used *pcd^{Sid}* mutants first recognized at Harvard Medical School (as described in [10]) and maintained by us as a congenic line on the same C57BL/6J background as the controls for more than 25 backcross generations. The homozygous *pcd^{Sid}* mutants were progeny of heterozygous parents or *pcd^{Sid}/pcd^{Sid}* females mated to +/*pcd^{Sid}* males. (Homozygous mutant males are almost completely sterile.) Wild-type and *pcd^{Sid}* mice were perfused through the heart with fresh 4% paraformaldehyde in phosphate-buffered saline (pH 7.4) at room temperature. Brains were dissected the next day from the cranium and kept in the same fixative at 4 $^{\circ}$ C until prepared for MRI study. Brains were then transferred into a 4% paraformaldehyde solution containing 1 mM gadolinium (Gd-DTPA) MRI contrast agent for at least 1 week to reduce the T1 relaxation time while ensuring that sufficient T2-weighted signal remains.

MRI Scan Parameters

During image acquisition, the brain specimens were placed in Fomblin solution (Ausimont, Thorofare, NJ) and scanned on a 9.4T Bruker Biospec MR system. The pulse sequence used for image acquisition was a 3D diffusion-weighted spin-echo echo-planar imaging sequence, TR 400 ms, TE 20 ms, number of segments 2, with an imaging matrix of $112 \times 112 \times 160$ pixels. Spatial resolution was $100 \times 100 \times 100 \mu\text{m}$. Sixty diffusion-weighted measurements ($b = 4000 \text{ s/mm}^2$) and one non-diffusion-weighted ($b = 0$) measurement were acquired, with $\delta = 12.0 \text{ ms}$, $\Delta = 24.2 \text{ m}$. The total acquisition time was 2 h and 10 min for each imaging session.

Diffusion Data Analyses—Tractography

We reconstructed orientation distribution function in each voxel with the HARDI method and reconstructed tractography pathways with a streamline algorithm for diffusion tractography [16]. The same approach was used in previous publications [12–15, 17, 18]. Trajectories were propagated by consistently pursuing the orientation vector of least curvature. Diffusion Toolkit and TrackVis (<http://trackvis.org>) were used to reconstruct and visualize tractography pathways. The color-coding of tractography pathways is based on a standard RGB code, applied to the vector between the end-points of each fiber (red: left-right, green: dorsal-ventral, blue: anterior-posterior).

We terminated tracking when the angle between two consecutive orientation vectors was greater than the given threshold (45°) for each specimen. We used a brain mask created by Diffusion Toolkit to terminate tracts as we explored the coherence in the brain, and not in the fluid in which we submersed the brain, so that the mask extracted the connectivity in the brain. We used mean diffusion-weighted images as mask images and excluded regions outside of the brain and inside of the ventricle. We used one mask image per brain and obtained whole-brain tractography pathways within the mask. As in previous studies in the mouse or rat [19, 20] and other species (e.g., [12–15, 21, 22]), no FA threshold was applied. In many tractography studies, fractional anisotropy (FA) values are used to terminate fibers in the gray matter which, in adults, has lower FA values than the white matter. However, as one of the objectives of our study was to detect fibers in abnormal brain areas that possibly have low FA regions, we used brain mask volumes to terminate tractography fibers instead of the FA threshold. This method was used previously [12] and is an acceptable alternate method [17, 18].

After reconstructing whole-brain pathways, cerebellar pathways were first identified in spherical regions of interest (ROIs) that included all cerebellar regions, and either a median sagittal (for Fig. 2 and upper panels of Fig. 4a, b) or an axial (for Fig. 3 and lower panels of Fig. 4a, b) slice filter was also

used to visualize specific pathways of interest. First, we used just one, large spherical ROI to identify all the cerebellar pathways and presented pathways in Figs. 2, 3, and 5 using one slice filter per brain. For Fig. 4, we used a mouse brain atlas to place additional spherical ROIs including the target anatomic structures. For a visualization purpose, 10% (Figs. 2c, g, 3c, and g) or 50% (Figs. 2d, h, 3d, h, and 4) of the total detected pathways using the slice filters were shown in each panel. Fiber tracking was first performed in the whole brain. We did not take anatomical (T1 or T2) images and used mean diffusion-weighted images to make ROIs. We also used slice filters to better show our results. The used spherical ROIs were initially made much larger than the size of the target anatomic structures, and by looking at tractography pathways running through the ROIs, we made the ROIs smaller, if necessary, carefully checking not to miss fibers from the target structures.

Results

Advanced Degeneration Stage (8 Months Old)

Whole-brain sagittal views (Fig. 2a, e) showed, overall, similar patterns of pathways between the mutants and controls. However, after magnifying cerebellar regions (white rectangles), clear differences were observed. Mean diffusion images showed clear folial anatomy in the control brain (Fig. 2b), whereas such folial structures were not clearly detected in the mutant brain (Fig. 2f). In accordance with past findings [10], the cerebellum was smaller in the mutant mice than in the normal mice, suggesting cell body, dendritic tree, and axonal fiber degeneration in the mutant cerebellum. Magnified tractography pathways in the control brain clearly identified red pathways running in the left-right direction within the gray matter (Fig. 2c, d), and green pathways in the dorsal-ventral direction (light blue arrows in Fig. 2a, c, d), between the red pathways, within the white matter. These pathways were in agreement with our previous study in adult human cerebellum [15]. The course and location of the red pathways (white arrows in Fig. 2a, c, d) correspond to regions where parallel fibers are located and green pathways in the white matter (light blue arrows in Fig. 2a, c, d) likely correspond to mossy fibers, climbing fibers, and axons of PNs coursing between cerebellar cortex and deep cerebellar nuclei. In the mutant brain, red and green pathways were disorganized with a lower number of fibers (there were almost no coherent green pathways, and red pathways were intermingled without repetitive coherent structures in Fig. 2g, h). In contrast, for example, corpus callosal pathways (green arrows in Fig. 2a, e) and middle cerebellar peduncles (yellow arrows in Fig. 2a, e) were similar in the control and mutant.

Figure 3 shows axial views of tractography pathways. Red pathways running in the right-left direction likely correspond

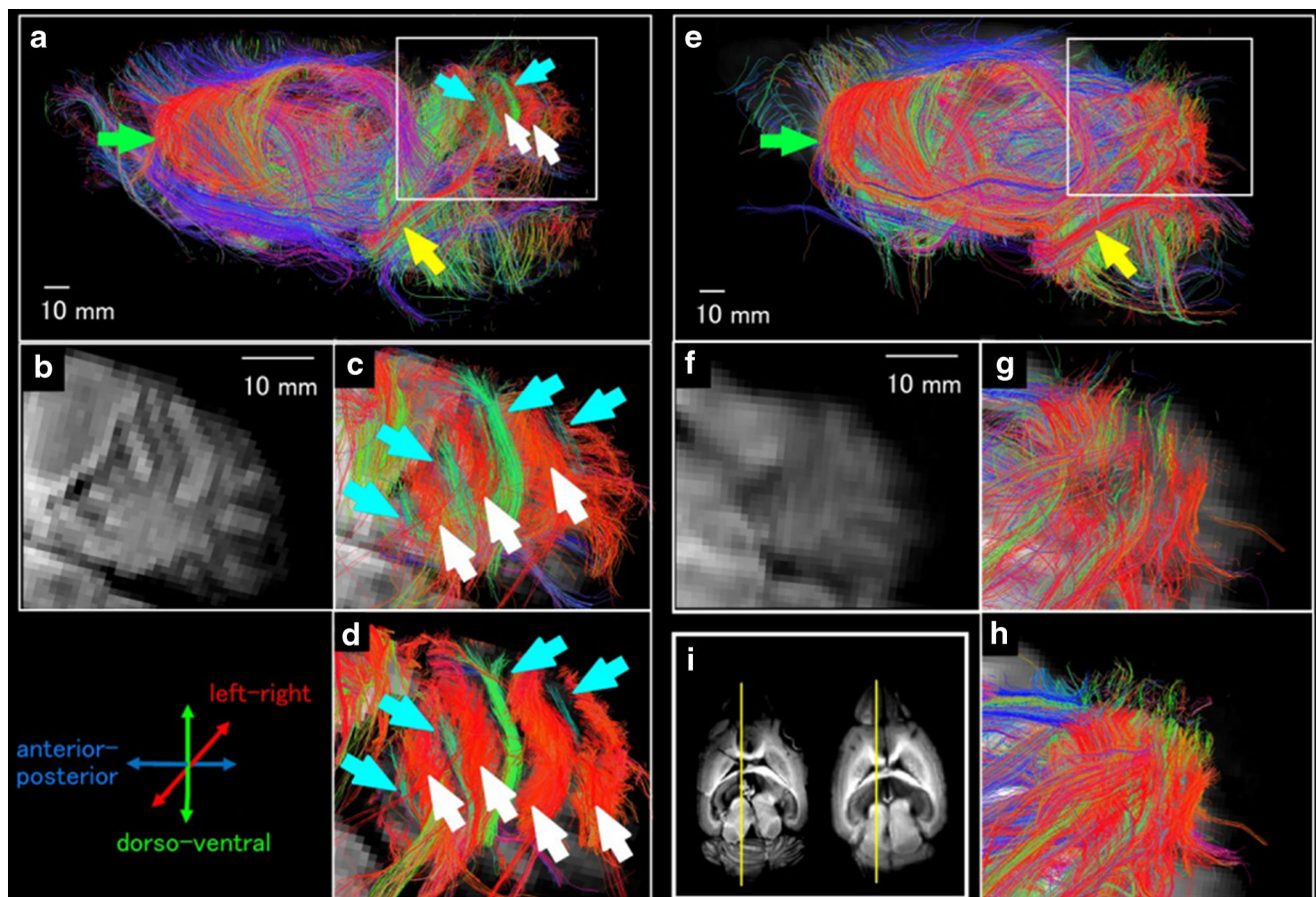


Fig. 2 Sagittal views of tractography pathways running through a median sagittal slice in a control (a–d) and a pcd^{Sid} mutant (e–h) mouse aged 8 months. The cerebellum (*white rectangle*) is located in the upper right in a and e. The anterior end of the corpus callosum pathways are indicated by *horizontal green arrows* (a, e), and the middle cerebellar peduncle by *large yellow arrows* (a, e). Magnified views of the cerebellum of the control (b–d) and mutant (f–h). i Axial slices of the control (*left*) and mutant (*right*) brains with yellow lines indicating the sagittal slices shown in a–d and e–h, respectively. Mean diffusion

weighted images are shown in b, f, i, and used under tractography pathways in the other panels. Ten percent of the total reconstructed tractography pathways are shown in c and g, and 50% in d and h for visualization purpose. Small *white arrows* in a and white arrows in c and d: red pathways likely corresponding to parallel fibers. *Light blue arrows* in a, c and d: green pathways in the white matter between the red pathways. The color-coding of tractography pathways is based on a standard RGB code, applied to the vector between the end-points of each fiber (*red*: left-right, *green*: dorsal-ventral, *blue*: anterior-posterior)

to parallel fibers running along folia (white arrows in Fig. 3a, c, d). Green fibers running in the dorsal-ventral direction between bundles of red pathways (light blue arrows in Fig. 3a, c, d) were found within the white matter and correspond to mossy fibers, climbing fibers, axons of PN, and cerebellar nucleo-cortical axons [15].

Pathways between the olfactory bulbs showed clear difference in the control and mutant brains (Fig. 4a, d). A region of interest was placed to cover the olfactory bulbs in both the left and right sides. Pathways between the olfactory bulbs were found to be a thick, coherent bundle in the control brain (white arrow in Fig. 4a), while in the mutant brain, there were only few pathways between the olfactory bulbs (white arrow in Fig. 4d). Pathways between the inferior colliculus and medial geniculate nucleus (Fig. 4b, e) and pathways between the medial geniculate nucleus and the cerebral cortex (Fig. 4c, f) took

similar projection courses between the control and mutant brains.

Early Degeneration Stage (20 Days Old)

Figure 5 shows sagittal and axial views of structural and tractography pathways of the cerebellum of a control (Fig. 5a, b) and a mutant (Fig. 5c, d) mouse brain at P20. In sagittal views, the cerebellum was detected to be smaller in the mutant (Fig. 5c) than in the control (Fig. 5a) while in axial views, the cerebellum was similar in size in both control and mutant mice (Fig. 5b, d). Compared to the 8-month-old mutant, folial structures in the P20 mutant were more preserved, especially in the axial view, although compared to the P20 control, tissue contrast was less clear overall in the mutant cerebellum, meaning there is lower signal in the gray matter

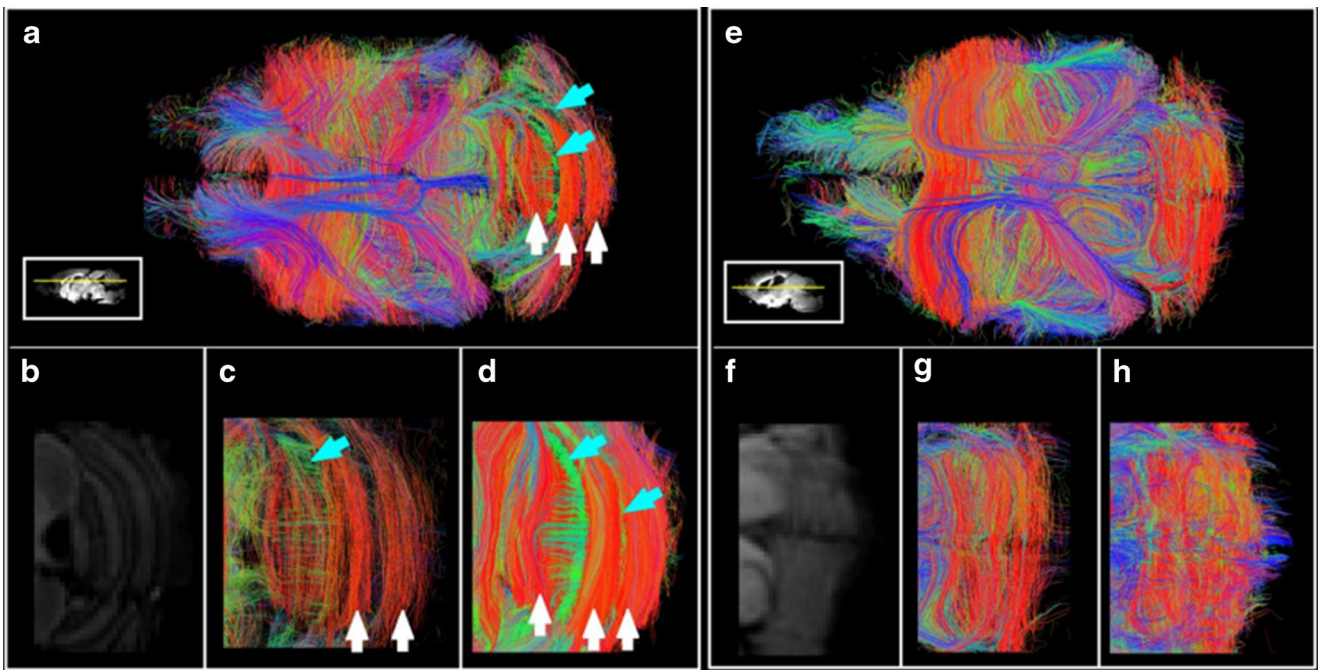
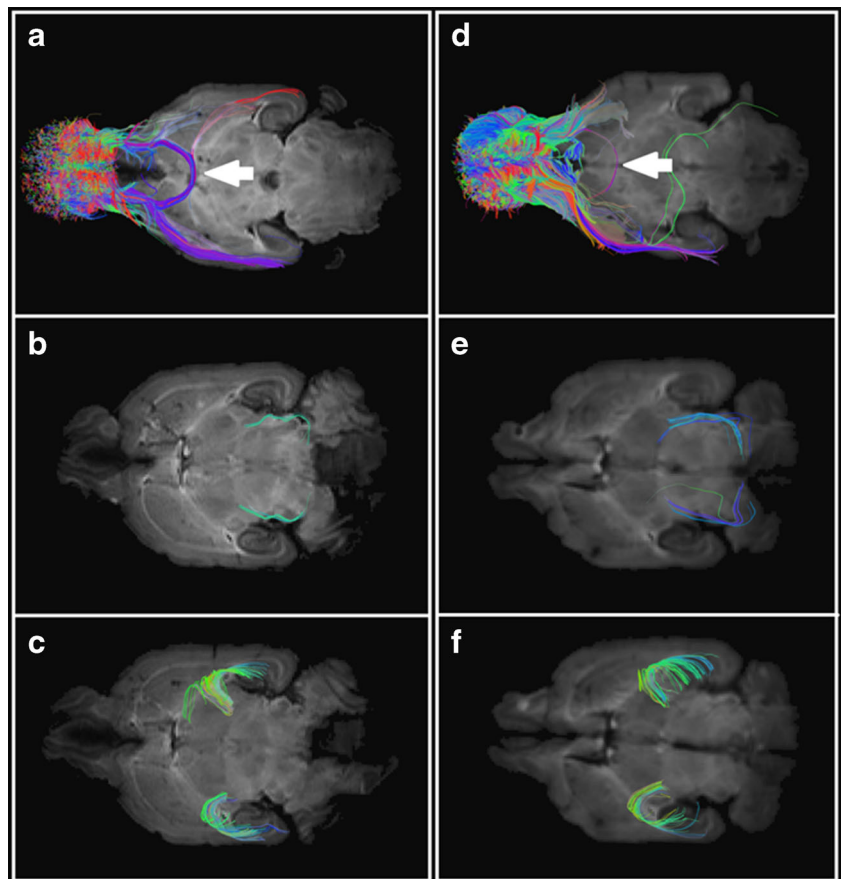


Fig. 3 Axial views of tractography pathways of the cerebellum in control (a–d) and mutant (e–h) mouse brains aged 8 months. Magnified views of the cerebellum of the control (b–d) and mutant (f–h). Mean diffusion weighted images are shown in b and f. *Small rectangle insertions* in a and e are sagittal slices with *yellow lines* indicating the level of axial slices shown in a–d and e–h, respectively. Ten percent of the total reconstructed

tractography pathways are shown in c and g, and 50% in d and h for a visualization purpose. *White arrows*: red pathways likely corresponding to parallel fibers. *Light blue arrows*: green pathways in the white matter between the red pathways. The color-coding of tractography pathways is based on a standard RGB code, as used in Fig. 1

Fig. 4 Pathways between olfactory bulbs (a, d), between the inferior colliculus and medial geniculate nucleus (b, e), and between the medial geniculate nucleus and the cerebral cortex (c, f) in control (a–c) and mutant (d–f) brains. The color-coding of tractography pathways is based on a standard RGB code, as used in Fig. 1



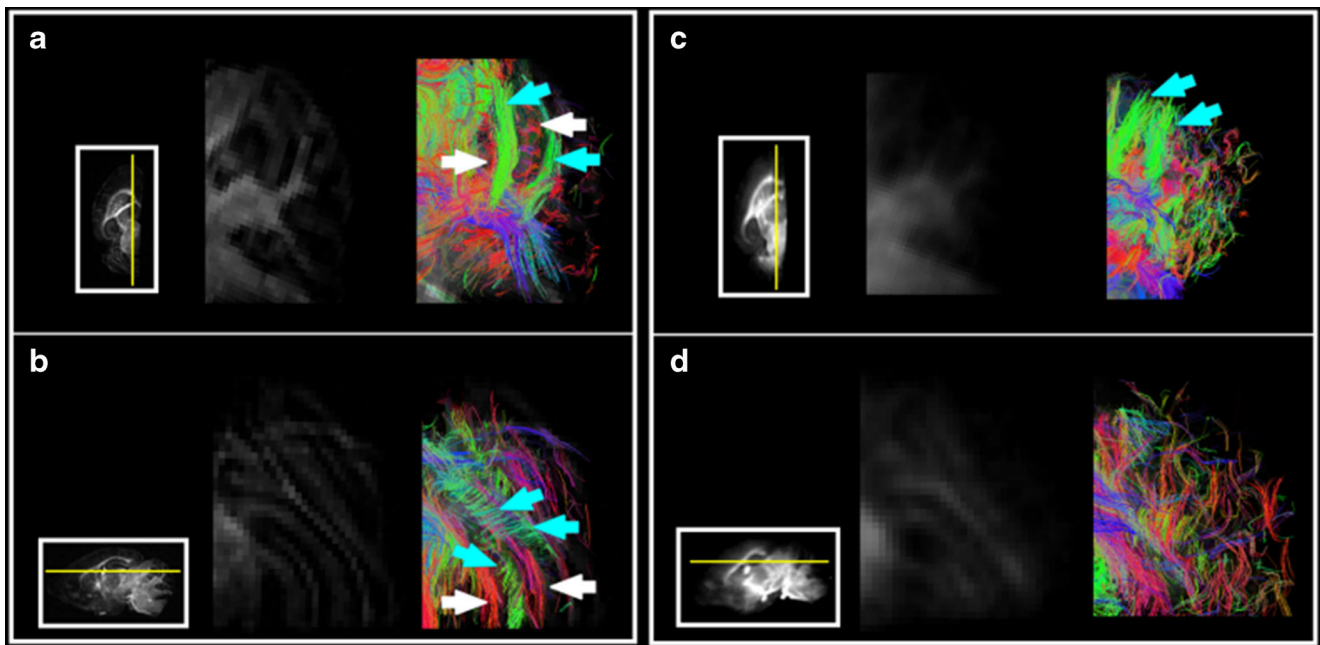


Fig. 5 Sagittal and axial views of tractography pathways of the cerebellum of a control (**a, b**) and a mutant (**c, d**) mouse brain aged 20 postnatal days. Sagittal (**a, c**) and axial (**b, d**) views are shown with *small rectangle insertions with yellow lines* (axial slice to show the sagittal level in **a** and **c** and sagittal slice to show the axial level in **b** and **d**). Fifty

percent of the total reconstructed tractography pathways are shown. *White arrows*: red pathways likely corresponding to parallel fibers. *Light blue arrows*: green pathways in the white matter between the red pathways. The color-coding of tractography pathways is based on a standard RGB code, as used in Fig. 1

of the cerebellum compared to that in the white matter in P20. Green pathways were running within the white matter (light blue arrows in Fig. 5a–c), and red pathways were running parallel to the folia (white arrows in Fig. 5a, b), corresponding to parallel fibers. No coherent red pathways were visible between the green pathways in the mutant brain (Fig. 5c, d) likely because degeneration of Purkinje cells had just begun and in the mutant, the cerebellar folia were already internally disorganized.

Discussion

In this study, we imaged abnormal structure and fiber pathways of a mouse model of Purkinje cell degeneration with high-angular resolution diffusion MR imaging (HARDI). Expected abnormalities, such as apparent reduction of the white matter volume [10], disorganized pathways likely linked to parallel fibers, mossy fibers, and other fibers running from/to the cerebellum (e.g., [15]) were observed in mutant mice. Such abnormalities were detected, not only in an advanced degeneration stage (mice 8 months old) but also in an early degeneration stage (P20). These results suggest that our diffusion MR tractography is useful for early detection of neuropathology in the cerebellum.

Overall Differences Between Mutants and Controls

The overall imaging contrast in mean diffusion folial MR images was very weak and unclear in the cerebellum of the *pcd* mutant mice, both at the early and advanced degeneration stages. By contrast, mean diffusion images from control mice showed organized, clear folial structures. The cerebellar size also appears much smaller in the *pcd* mutant compared to control mice in sagittal view. This is consistent with findings in past papers where the *pcd* mutant cerebellum was found to be smaller when using histopathology [10]. These results are in strong agreement with the summary by Sarna and Hawkes [2] that Purkinje cell death resulted in reduced cerebellar volume and loss of foliation, even at the early phase of PN degeneration.

Advanced Degeneration Stage

At the advanced degeneration stage (8 months old), while the middle cerebellar pathways were clearly detected in both mutant and control brains, specific local pathways likely linked to parallel fibers (red pathways in Figs. 2, 3, 4, and 5) and other fibers coursing radial to the parallel fibers in the white matter (green pathways in Figs. 2, 3, 4, and 5) [15] were apparently disorganized in the *pcd* mutant mice. Given the quality of the mean diffusion images in Fig. 2i, it is not likely that

disorganized tractography pathways are confound of poor anatomical identifications in the mutant mice. Significant decrease in red pathways and no green pathways running in the dorsal-ventral direction indicate the loss of parallel fibers (red pathways), mossy fibers, climbing fibers, axons of PNs, and other pathways along them (green pathways) [14, 15] that were likely caused by the degeneration of Purkinje cell bodies and dendrites.

Pathways between left and right olfactory bulbs were found to be significantly reduced in number in the mutant brain compared to the control brain, which agrees with past findings on degeneration of olfactory bulb mitral neurons [23, 24].

Given that the ventral medial geniculate nucleus of the thalamus degenerates severely between P50–P60 [25, 26], one may ask whether the presynaptic fiber tract from the inferior colliculus to the medial geniculate nucleus may have lost its fibers. Such axonal loss was not seen in the earlier studies, and the tractography pathways between the inferior colliculus and medial geniculate nucleus were not different in number or trajectory between the control and mutant brains. Also, the extensive thalamocortical axonal degeneration in the tract from the medial geniculate nucleus to the auditory region of the cerebral cortex [25] was not seen in the HARDI tractography images. Among the potential reasons why tractography did not detect auditory thalamocortical tracts degeneration include the relatively small size and low density of these tracts. Javad and colleagues argued about the difficulty to identify auditory fiber pathways by using diffusion tractography [27]. They discussed that due to known limitations of diffusion MRI in resolving multiple fiber pathways in each voxel [28, 29], the technique limited its application in the identification of the auditory white matter pathways, mentioning that the auditory radiation is particularly susceptible to this problem due to its small size and to its crossing, along its path, with larger fascicles such as the corticospinal tracts and the optic radiation.

Early Degeneration Stage

At the early degeneration stage (P20), red tractography pathways were not detected, while green pathways were still clearly observed. Given that both the red and green pathways were apparently disorganized in the advanced stage, and the *pcd* disease was known to be PN-autonomous [24, 30], one may speculate that the decreased input from parallel fibers to dendrites of PNs [4] may be an early consequence close to the time of onset of Purkinje cell degeneration. Given that green tractography pathways were still detected at this stage and that there is no method currently to differentiate the green pathways further into mossy fiber, climbing fiber, PN axon, and other sub-pathways between deep cerebellar nuclei and cerebellar cortex, future studies should explore how to use MRI to differentiate between sub-pathways connecting deep

cerebellar nuclei and cerebellar cortex in order to do additional detailed 3D imaging during PN degeneration.

Limitation of the Current Study and Future Directions

We are aware that our sample size is small. However, many of our findings were in strong agreement with past studies [10, 31–33], with HARDI data on specific types of pathways (e.g., intact middle cerebellar peduncle versus disorganized pathways for parallel fibers with other disorganized local white matter pathways), indicating that this technique can serve for further detection of long-range fiber pathway differences between pathological and control nervous system specimens. Given that studies on mouse models of Purkinje cell degeneration have suggested that such mutant mice might have aberrant or degenerated fiber pathways between the cerebellum and cerebrum cortices [9, 25, 34], future imaging research would focus on detecting such pathologies in the cerebral cortex. Along the cerebro-cerebellar pathways, there are extensive fiber crossings in the pons and midbrain and our technique did not identify reasonable anatomic pathways continuous between the cerebellum and cerebrum.

Although we detected pathways that correspond to large bundles of closely packed parallel fibers that are unmyelinated and often less than 1 μm in diameter, and other more heterogeneous pathways running radial to the parallel pathways toward the cerebellar surface, we did not detect pathways linked to axons of cerebellar cortical interneurons (mostly stellate cells) that were detected in our former study in adult humans [15], in neither the controls nor the mutants. Such axons of cortical interneurons were detected to be perpendicular to both pathways and linked to parallel fibers, climbing fibers, and others in humans. A higher spatial resolution may be necessary to image such pathways in mouse brains [35, 36].

Acknowledgments This work was supported by Boston Children's Hospital and NIH (R01HD078561, R21HD069001, R03NS091587) (ET). The authors thank Guangping Dai for technical advice and Natalie Stewart for editorial assistance.

Compliance with Ethical Standards All procedures were in accordance with NIH-approved institutional guidelines maintained by the Institutional Animal Care and Use Committee of Harvard Medical School and the University of Connecticut.

Conflict of Interest The authors declare that there are no conflicts of interest.

References

1. Ichise T, Kano M, Hashimoto K, Yanagihara D, Nakao K, Shigemoto R, Katsuki M, Aiba A. mGluR1 in cerebellar Purkinje cells essential for long-term depression, synapse elimination, and motor coordination. *Science*. 2009;288(5472):1832–4.

2. Sarna JR, Hawkes R. Patterned Purkinje cell death in the cerebellum. *Prog Neurobiol*. 2003;70:473–507.
3. Thatch W. A role for the cerebellum in learning movement coordination. *Neurobiol Learn Mem*. 1998;70(1–2):177–88.
4. Kapfhammer JP. Cellular and molecular control of dendritic growth and development of cerebellar Purkinje cells. *Prog Histochem Cytochem*. 2004;39:131–82.
5. Mavroudis IA, Fotiou DF, Adipepe LF, Manani MG, Njau SD, Psaroulis D, Costa VG, Baloyannis SJ. Morphological changes of the human Purkinje cells and deposition of neuritic plaques and neurofibrillary tangles on the cerebellar cortex of Alzheimer's disease. *Am J Alzheimers Dis Other Dement*. 2010;25:585–91.
6. Rogers TD, McKimm E, Dickson PE, Goldowitz D, Blaha CD, Mittleman G. Is autism a disease of the cerebellum? An integration of clinical and pre-clinical research. *Front Systems Neurosci*. 2013;7:15.
7. Sirzen-Zelenskaya A, Zeise J, Kapfhammer JP. Activation of class I metabotropic glutamate receptors limits dendritic growth of Purkinje cells in organotypic slice cultures. *Eur J Neurosci*. 2006;24:2978–86.
8. Fernandez-Gonzalez A, La Spada AR, Treadaway J, Higdon JC, Harris BS, Sidman RL, Morgan JI, Zuo J. Purkinje cell degeneration (pcd) phenotypes caused by mutations in the axotomy-induced gene, *Nna1*. *Science*. 2002;295:1904–6.
9. Wang T, Morgan JI. The Purkinje cell degeneration (pcd) mouse: an unexpected molecular link between neuronal degeneration and regeneration. *Brain Res*. 2007;1140:26–40.
10. Li J, Gu X, Ma Y, Calicchio ML, Kong D, Teng YD, Yu L, Crain AM, Vartanian TK, Pasqualini R, Arap W, Libermann TA, Snyder EY, Sidman RL. *Nna1* mediates Purkinje cell dendritic development via lysyl oxidase propeptide and NF- κ B signaling. *Neuron*. 2010;68:45–60.
11. Tuch DS, Reese TG, Wiegell MR, Wedeen VJ. Diffusion MRI of complex neural architecture. *Neuron*. 2003;40:885–95.
12. Takahashi E, Dai G, Rosen GD, Wang R, Ohki K, Folkerth RD, Galaburda AL, Wedeen VJ, Grant PE. Developing neocortex organization and connectivity in cats revealed by direct correlation of diffusion tractography and histology. *Cereb Cortex*. 2011;21:200–11.
13. Takahashi E, Folkerth RD, Galaburda AL, Grant PE. Emerging cerebral connectivity in the human fetal brain: an MR tractography study. *Cereb Cortex*. 2012;22:455–64.
14. Takahashi E, Hayashi E, Schmahmann JD, Grant PE. Development of cerebellar connectivity in human fetal brains revealed by high angular resolution diffusion tractography. *NeuroImage*. 2014;96:326–33.
15. Takahashi E, Song JW, Folkerth RD, Grant PE, Schmahmann JD. Detection of cerebellar cortex and white matter pathways using high angular resolution diffusion tractography. *NeuroImage*. 2013;68:105–11.
16. Mori S. Introduction to diffusion tensor imaging. 1st ed. Oxford: Elsevier Science; 2007.
17. Schmahmann JD, Pandya DN, Wang R, Dai G, D'Arceuil HE, de Crespigny AJ, Wedeen VJ. Association fibre pathways of the brain: parallel observations from diffusion spectrum imaging and autoradiography. *Brain*. 2007;130:630–53.
18. Wedeen VJ, Wang RP, Schmahmann JD, Benner T, Tseng WY, Dai G, et al. Diffusion spectrum magnetic resonance imaging (DSI) tractography of crossing fibers. *NeuroImage*. 2008;41(4):1267–77.
19. Lodato S, Molyneaux BJ, Zuccaro E, Goff LA, Chen H-H, Yuan W, Meleski A, Takahashi E, Mahony S, Rinn JL, Gifford DK, Arlotta P. Gene co-regulation by *Fezf2* selects neurotransmitter identity and connectivity of corticospinal neurons. *Nat Neurosci*. 2014;17:1046–54.
20. Rosen GD, Azoulay NG, Griffin EG, Newbury A, Koganti L, Fujisaki N, Takahashi E, Grant PE, Truong DT, Fitch RH, Lu L, Williams RW. Bilateral subcortical heterotopia with partial callosal agenesis in a mouse mutant. *Cereb Cortex*. 2013;23:859–72.
21. Song JW, Mitchell PD, Kolasinski J, Ellen Grant P, Galaburda AM, Takahashi E. Asymmetry of white matter pathways in developing human brains. *Cereb Cortex*. 2015;25:2883–93.
22. Takahashi E, Dai G, Wang R, Ohki K, Rosen GD, Galaburda AL, Grant PE, Wedeen VJ. Development of cerebral fiber pathways in cats revealed by diffusion spectrum imaging. *NeuroImage*. 2010;49:1231–40.
23. Greer CA, Shepherd GM. Mitral cell degeneration and sensory function in the neurological mutant mouse Purkinje cell degeneration (PCD). *Brain Res*. 1982;235(1):156–61.
24. Mullen RJ, Eicher EM, Sidman RL. Purkinje cell degeneration, a new neurological mutation in the mouse. *Proc Natl Acad Sci U S A*. 1976;73(1):208–12.
25. O'Gorman S, Sidman RL. Degeneration of thalamic neurons in "Purkinje cell degeneration" mutant mice. I. Distribution of neuron loss. *J Comp Neurol*. 1985;234:277–97.
26. O'Gorman S. Degeneration of thalamic neurons in "Purkinje cell degeneration" mutant mice. II Cytology of neuron loss *J Comp Neurol*. 1985;234(3):298–316.
27. Javad F, Warren JD, Micallef C, Thornton JS, Golay X, Yousry T, Mancini L. Auditory tracts identified with combined MRI and diffusion tractography. *NeuroImage*. 2014;84(100):562–74.
28. Behrens TEJ, Johansen-Berg H, Woolrich MW, Smith SM, Wheeler-Kingshott CAM, Boulby PA, Barker GJ, Sillery EL, Sheehan K, Ciccarelli O, Thompson AJ, Brady JM, Matthews PM. Non-invasive mapping of connections between human thalamus and cortex using diffusion imaging. *Nat Neurosci*. 2003;6(7):750–7.
29. Seurinink KK, Alexander DC. (2009). Multiple fibers: beyond the diffusion tensor. *Diffusion MRI: from quantitative measurement to in vivo neuroanatomy*, Academic Press. 55–72.
30. Mullen RJ. Site of *pcd* gene action and Purkinje cell mosaicism in cerebella of chimaeric mice. *Nature*. 1977;270(5634):245–7.
31. Carletti B, Rossi F. Neurogenesis in the cerebellum. *Neurosci*. 2008;14:91–100.
32. Dusart I, Guenet JL, Sotelo C. Purkinje cell death: differences between developmental cell death and neurodegenerative death in mutant mice. *Cerebellum*. 2006;5:163–73.
33. Goldowitz D, Hamre K. The cells and molecules that make a cerebellum. *Trends Neurosci*. 1998;21:375–82.
34. Landis SC, Mullen RJ. The development and degeneration of Purkinje cells in *pcd* mutant mice. *J Comp Neurol*. 1978;177:125–43.
35. Alomair OI, Brereton IM, Smith MT, Galloway GJ, Kurniawan ND. In vivo high angular resolution diffusion-weighted imaging of mouse brain at 16.4 tesla. *PLoS One*. 2015;10:e0130133.
36. Zhang J, Jones M, DeBoy CA, Reich DS, Farrell JA, Hoffman PN, Griffin JW, Sheikh KA, Miller MI, Mori S, Calabresi PA. Diffusion tensor magnetic resonance imaging of Wallerian degeneration in rat spinal cord after dorsal root axotomy. *J Neurosci*. 2009;29(10):3160–71.